Water Resources Research

RESEARCH ARTICLE
10.1029/2020WR027304

Dual-Permeability Model Improvements for Representation of Preferential Flow in Fractured Clays

Juan P. Aguilar-López[1,2], Thom Bogaard[2], and Horst H. Gerke[3]

[1]Department of Hydraulic Engineering, Faculty of Civil Engineering and Geosciences, Delft University of Technology, Delft, Netherlands, [2]Department of Water Resources Management, Faculty of Civil Engineering and Geosciences, Delft University of Technology, Delft, Netherlands, [3]Working group "Hydropedology"-Research Area 1 "Landscape functioning", Leibniz Centre for Agricultural Landscape Research (ZALF) e.V., Müncheberg, Germany

Key Points:
- Dual-permeability model improvement for modeling wide fractures by reformulating the α parameter in the Mualem-van Genuchten model soil water retention curve (SWRC)
- Rigorous evaluation of the dual-permeability interface mass exchange function
- SWRC exponent n sensitivity analysis for dual-permeability model

Correspondence to:
J. P. Aguilar-López;
j.p.aguilarlopez@tudelft.nl

Citation:
Aguilar-López, J. P., Bogaard, T., & Gerke, H. H. (2020). Dual-permeability model improvements for representation of preferential flow in fractured clays. *Water Resources Research*, *56*, e2020WR027304. https://doi.org/10.1029/2020WR027304

Received 3 APR 2020
Accepted 29 JUN 2020
Accepted article online 6 JUL 2020

©2020. The Authors.
This is an open access article under the terms of the Creative Commons Attribution-NonCommercial-NoDerivs License, which permits use and distribution in any medium, provided the original work is properly cited, the use is non-commercial and no modifications or adaptations are made.

Abstract Dual-permeability models assume that the complete porous media system can be represented by two different interacting subsystems: the matrix and the fracture pore domain. For some soils like fractured clays, the fracture domain may be empty, which makes its physical behavior differ significantly from capillary flow. Our main hypothesis is that this kind of preferential flow systems can be represented as a dual-permeability porous media by adapting the 2-D formulation and initial conditions of the fracture domain and the mass exchange function. The performance of the dual-permeability finite element solution was evaluated by comparing it to its equivalent 2-D explicit fracture single-permeability finite element model. The results of the numerical experiments show that the 2-D dual-permeability concept allows to simulate preferential flow in soils with fractures. This was achieved by improving the parameterization of the Mualem-van Genuchten soil water retention curve of the fractured domain and the hydraulic conductivity exchange function for the first-order mass exchange term for fractured soils. The exchange term hydraulic conductivity evaluated at the minimum value of the pressure heads of the two domains considerably improved the results as compared to using the well-established arithmetic average of the hydraulic conductivity values from both domains. These two improvements of the dual-permeability model approach are especially useful in cases where preferential flow systems consist mostly of relatively large, noncapillary fractures and macropores.

1. Introduction

Preferential flow due to presence of fractures occurs in the most permeable regions of the porous media and has a big influence on the pressure head spatial distribution and fluxes inside the soil. In standard porous media simulations, preferential flow paths (e.g., macropores and fractures) are "disguised" by the averaging of the permeability properties in space (Hendrickx & Flury, 2001). In fact, this is the basis of the Darcian flow solutions (Whitaker, 1986), for which characteristics like porosity and permeability are averaged inside the REA (representative elementary area when 2-D Bear, 1972) to be modeled. For clay soils with fractures, the presence of preferential flow paths highly influences the flow dynamics in terms of infiltration and water retention (Drumm et al., 1997; Li et al., 2011; Novak et al., 2000). Therefore, the challenge remains in finding the best way to model water movement in soils dominated by macropores that cannot be included by averaging nor fit in the capillary modeling concept. There are several studies that aim at developing this type of models (Pouya, 2015; Pouya et al., 2019; Walton et al., 2019), but their implementation requires explicit dense discretization of the matrix and fractures domains mesh, making them computationally unfeasible for representing systems which are larger than a few fractures.

Dual-porosity (DPoM) and dual-permeability (DPM) model conceptualizations have proven to be capable of representing the equilibrium, nonequilibrium, and water exchange between fractures and matrix for different types of preferential flows (Šimůnek et al., 2003). The DPM concept in particular has been widely used for modeling fractured rock (Barenblatt et al., 1960), reservoir simulations (Moinfar et al., 2011), and two-dimensional contaminant transport (Dykhuizen, 1987; Vogel, Gerke, et al., 2000). This type of models assumes that the system can be represented as two overlapping interacting regions, one which represents an interaggregate fractured or mesoporous media and the other one which represents an intra-aggregate meso-micro pore type of subsystem. Both permeable and less permeable subsystems are solved

simultaneously as porous media continuum models. Hence, fractured clays become a great challenge for DPM as the fracture subsystem behaves more similar to a fluid pressurized conduit rather than a porous media. For these cases, Darcian flow approximations for estimating laminar fluxes inside small conduits have been studied and implemented in porous media simulation in the past (e.g., Aguilar-López et al., 2016; Oron & Berkowitz, 1998; Snow, 1965; 1969; Witherspoon et al., 1980, and others). This approximation allowed to reduce the computational burden from coupling Darcian numerical solutions (matrix subsystem) to a Navier-Stokes type of numerical solutions (macropore flow). In addition, explicit fracture models (EMs) require to define the geometrical and hydraulic properties of the fractures locally, making them unfeasible for simulating systems larger than few fractures.

Regarding the water retention models of macropore-dominated systems, methods for constructing composite soil water retention curves (SWRC) also aimed to reduce complexity required for solving two coupled Richards equation systems (Chertkov & Ravina, 2001; Li et al., 2009). Specifically for fractured clays, Fredlund et al. (2010) tackled preferential flow modeling by implementing the superposition of the SWRC of matrix and fracture flow subsystems. While these kinds of approaches are capable of capturing the capillary effects derived from partially saturated fractured soils, they are still not capable of estimating the dynamic exchange of mass between soil and fracture subsystems in time.

This mass exchange term and its modeling has been studied by Samardzioska and Popov (2005) and Moinfar et al. (2011), who confirmed their accuracy for both oil and water flux in fractured mediums. Furthermore, its numerical approximation (Ebel et al., 2009; Gerke & van Genuchten, 1993b; Köhne et al., 2004, Köhne et al., 2009) and its geometrical conceptualization (Gerke & van Genuchten, 1996) has also been studied for DPM. All of them gave special attention in determining the correct exchange function to ensure a logical hydrological response in the simulated system. While all previous studies validated their approaches, all of them assumed the fractured subsystem to be composed not only of macropores but of other hetereogenities as well (e.g., soil blocks, roots, and pebbles). This makes them easier to be represented by conventional water retention models like Brooks and Corey (1966) or van Genuchten (1980). However, for macropore-dominated soils, the fractured subsystem must be conceptualized as a completely hollow space. One of the common approaches is to parameterize this subsystem as an extremely low capillarity rise medium (e.g., a wide fracture). This is done by assuming a wide fracture aperture value in the capillary rise Young-Laplace relation for parallel plates (Adam, 1930). However, this results in a large value of the (α) in the SWRC which leads to the contrary of the desired effect: a less permeable soil from a numerical point of view. This was originally pointed out by Wang and Narasimhan (1985), who showed that this kind of parameterizations results in extreme dry initial soil moisture conditions. The dual-porosity concept for describing preferential flow and local nonequilibrium conditions has often been criticized as too empirical because it relies on the Richards equation, which has been found useful but physically not adequate representation of flow in a heterogeneous unsaturated soil (Beven & Germann, 2013). In addition, DPoM parameters can be determined mainly by fitting. Hence, the theoretical problem of choosing effective values at the scales of interest remained unresolved (Beven & Germann, 2013). Alternative approaches such as Stokes flow (Germann & Karlen, 2016) or particle tracking may provide integrated ways of incorporating preferential flows at larger scales but at the expense of neglecting capillarity (Beven, 2018).

Since the capillary effects become less important as fractures become wider, the desired faster infiltration effect is better represented by means of purely fluid flow type of physical equations. The MACRO model proposed by Jarvis (1994), for example, approximates the fracture domain flux behavior to a kinematic wave type of flow rather than a Darcian one. As a side effect, the kinematic wave approximation reduces the number of required parameters in the preferential flow domain as it does not require any water retention model parameterization. The drawback from this model is that it only considers a 1-D vertical gravity driven flow for the macropore domain (Šimůnek et al., 2003), which is not fully representative for fractured soil systems with preferential flow paths in multiple directions.

The main hypothesis for this study is that the DPM may be used to simulate soils for which the fracture domain represents a single macropore flowing in laminar flow conditions. This will not only reduce the computational burden required for the solution of single-permeability models with explicit fractures, but it will also avoid the need of the geometrical characterization of the fractures. Hence, the objective of this study is to test the performance of the 2-D DPM concept presented by Vogel, Gerke, et al. (2000) for representing soils

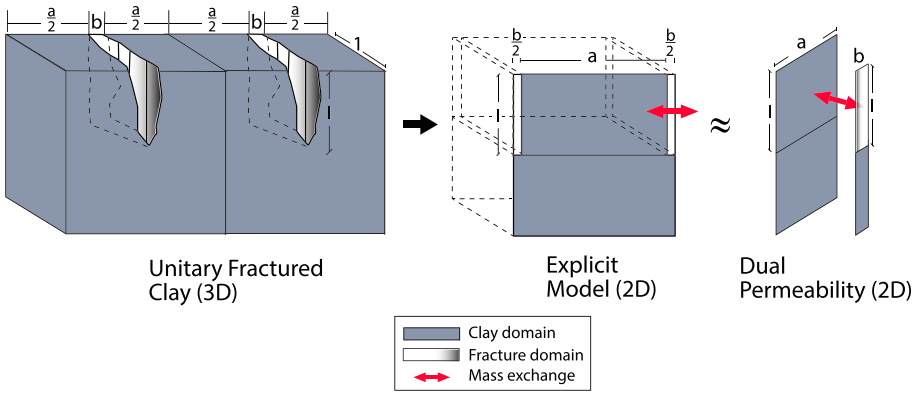

Figure 1. Dual-permeability model conceptualization.

with large open fractures. Note that the DPM concept was originally formulated by Gerke and van Genuchten (1993a) as a 1-D problem and aimed to better represent soils with preferential flows in general. In the present study we propose four things that improved the original concept for representing fractured clays. These improvements were done in terms of parameterization and representation of the mass exchange between matrix and fracture subdomains. They consist of the following:

1. Evaluating the saturated hydraulic conductivity of the fracture subsystem based on the "cubic law" (Snow, 1965; Witherspoon et al., 1980).
2. Reformulating of the α parameter of the SWRC of the fracture subsystem so that the residual water content is achieved for a pressure head value close to the initial condition of the simulation.
3. Redefining the mass transfer hydraulic conductivity function between matrix and fracture subsystems, with respect to the original DPM concept based on other existent models.
4. Recommending a semifixed n exponent value for wide fractures of the SWRC based on a sensitivity analysis.

Section 2 explains how the EM was used to evaluate the performance of the DPM. Hereafter in section 3, it is explained how the DPM fracture subsystem was adapted to represent a single-macropore representative domain. In section 4, the DPM model setup and different numerical experiments to evaluate the adapted DPM to represent the EM model are explained. The results from all numerical experiments are explained in section 5 and discussed in section 6, and finally the conclusions from the study are summarized in section 7.

2. EM Versus DPM

The performance of the DPM modifications are evaluated by comparing its simulation results with respect to the ones obtained from an analogous single-permeability model of a fractured block of clay (EM). The EM is a model in which the fractures are explicitly included as highly permeable domains for which their SWRC is parameterized (Figure 1, second block).

The DPM is an approximation of the EM REA without having to explicitly include the fractures but representing them as an overlapping domain (Figure 1, third block).

2.1. EM

The EM is simulated by solving the 2-D Richards' equation in its head based form (Celia et al., 1990) as

$$C(h)\frac{\partial h}{\partial t} = \nabla[K(h)\nabla(h+z)] \tag{1}$$

where (h) (m) is the pressure head, (C) represents the specific water capacity $(d\theta/dh)$ (1/m), (θ) (m^3/m^3) is the volumetric water content, (K) (m/s) is the hydraulic conductivity, and (z) (m) is the elevation head. The hydraulic properties per type of soil are parameterized based on the Mualem-van Genuchten water SWRC (Mualem, 1976; van Genuchten, 1980) as

$$S_e(h) = [1+(|\alpha h|)^n]^{-m} = \frac{\theta - \theta_r}{\theta_s - \theta_r} \tag{2}$$

$$K(S_e) = K_s S_e^{0.5}[1-(1-S_e^{1/m})^m]^2 \tag{3}$$

(S_e) (–) is the effective saturation, (θ_s) (m^3/m^3) is the saturated water content, (θ_r) (m^3/m^3) is the residual volumetric water content, (α) (1/m) is a scaling fitting parameter, (n) and (m) (–) are fitting parameters associated with the pore distribution ($m = 1-1/n$) for Mualem-van Genuchten), and ($K(S_e)$) (m/s) is the estimated hydraulic conductivity as a function of the relative water saturation.

2.2. DPM

The DPM concept used in this study corresponds to the one presented by Gerke and van Genuchten (1993a). Here, the soil matrix domain is denoted with the subscript letter (m), the fracture representative domain is denoted with the subscript letter (f), and they are related to each other as

$$w_m + w_f = 1 \tag{4}$$

The (w_f) and (w_m) are the volumetric ratios of fracture and matrix from the soil REA. They are estimated from the top projection where the fracture aperture is located (Figure 1). making their summation equal to the unity ensures that the total water content of both superimposed systems remains equal to the total volumetric content of its equivalent single-permeability system. Hence, its total porosity (ε) (m^3/m^3), total moisture content (θ) (m^3/m^3), and total volumetric flux (q) (m/s) in terms of both subsystems can be expressed as

$$\varepsilon = w_m\varepsilon_m + w_f\varepsilon_f \tag{5}$$

$$\theta = w_m\theta_m + w_f\theta_f \tag{6}$$

$$q = w_m q_m + w_f q_f \tag{7}$$

For the case of fractured clays, (w_f) is assumed to be equivalent to the superficial fracture porosity (n_c) (m^3/m^3) (Li & Zhang, 2010). This porosity is defined as the ratio between the superficial fracture (void) area with respect to the total soil area. For the present study, the value of (w_f) is set to 0.02 for all REAs in all experiments. This value is presented as a feasible average value for clays by Li and Zhang (2010).

The hydraulic conductivity (K) (m/s) of the single permeability can be related to the equivalent dual-permeability system as

$$K = w_m K_m + w_f K_f \tag{8}$$

Based on all previous volumetric equivalences, the DPM can be represented by a set of two Richards' 2-D formulations (Gerke et al., 2007; Vogel, Gerke, et al., 2000) as shown in Equations 9 and 10, which are coupled by the additional scaled exchange term (Γ_w) as

$$C_f(h)\frac{\partial h_f}{\partial t} = \nabla[K_f(h)\nabla(h_f + z)] - \frac{\Gamma_w}{w_f} \tag{9}$$

$$C_m(h)\frac{\partial h_m}{\partial t} = \nabla[K_m(h)\nabla(h_m + z)] + \frac{\Gamma_w}{w_m} \tag{10}$$

$$\Gamma_w = \alpha_w^* K_a(h_f - h_m) \tag{11}$$

$$\alpha_w^* = \frac{\beta\gamma_w}{a^2} \tag{12}$$

where (Γ) (1/s) is the exchange term between fracture and matrix domain. It is driven by the head difference between the two domains. The interface hydraulic conductivity is (K_a) (m/s), and (α_w^*) (m/s) is the first-order exchange coefficient. This last coefficient is determined by a combination of the (β)

dimensionless factor which depends on the shape of the aggregates, the (γ_w) dimensionless "scaling" coefficient (equal to 0.4; see Gerke et al., 2007), and a scaling factor (a) (m) which is approximated to half width of the average matrix block size (see Figure 1).

3. DPM for Single-Macropore Subsystems

Regarding the SWRC, the Mualem-van Genuchten model presented in Equations 2 and 3 is used for characterizing both the fracture and matrix domains. Yet, for the fracture domain, it is necessary to modify the parameterization so that this subsystem responds more similarly to a noncapillary conduit. The main goal here is to reduce the inner friction as much as possible to obtain faster flows inside the porous medium while having a relation between this resistance and the fracture geometry. In our case, for the fractures in clay, we assumed the macropore geometry as a flat rectangular aperture between clay blocks (see Figure 1). Based on this choice, we propose the following modifications on the original DPM concept so that we can approximate the DPM Richards equation behavior, to the expected one of a free flowing macropore.

3.1. Saturated Hydraulic Conductivity of the Fracture Domain (K_f)

Based on the derivation of laminar flow between parallel plates for Hagen-Poiseuille type of flow, a relation to the cubes of the aperture of a fracture with respect to the fracture inner flux was proposed by Snow (1965). Equating this same flux relation to the flux in Darcy's law, it is possible to obtain the approximated hydraulic conductivity inside a fracture with no tortuosity as

$$K_3 = \frac{b^2 g}{12\nu} \tag{13}$$

where (b) (m) stands for the fracture aperture length (see Figure 1), (g) (m/s^2) is the gravitational acceleration constant, and (ν) (m^2/s) is the water kinematic viscosity. For both EM and DPM, the fully saturated hydraulic conductivity of the fracture subsystem K_{s_f} is set equal to K_3.

3.2. SWRC Parameterization for a Single Macropore

3.2.1. Fracture θ_s and θ_r

For recreating the expected physical behavior of a fracture, the saturated water content θ_s is set equal to 0.99, and the residual water content θ_r is equal to 0.01, so that it can be saturated or dried. As the fracture flow is estimated using the Richards equation, it must be parameterized in terms of its SWRC (Equations 2 and 3) as well.

3.2.2. Fracture α Parameter

One of the most commonly used water retention models is the Brooks-Corey (Brooks & Corey, 1966). In this model, the air entry pressure parameter is directly related to the minimum capillary rise h_c. It is often misunderstood that the inverse of the air entry coefficient from Brooks-Corey is equivalent to the α parameter of the Mualem-van Genuchten SWRC (Equation 2). This common misconception was also pointed out by Vogel, van Genuchten, and Cislerova (2000) and more recently by van Lier and Pinheiro (2018). We wanted to test the implications of this error as well, and so we set the α parameter (Equation 2) to be equal to the reciprocal of the minimum capillary rise (h_c) between two parallel plates. This is calculated by assuming a distance equal to the average fracture aperture equal to b and replacing it in the Young-Laplace capillary rise relation as

$$\alpha = \frac{1}{h_c} = \frac{b\rho g}{(2\tau)\cos(\varphi)} \tag{14}$$

where (τ) (N/m) corresponds to the surface tension of water and (φ) is the water-air contact angle which is assumed equal to 0 in this study. By estimating α in this way, it is expected that large values of b will result in large values of K_f (Equation 13) and small values h_c (Equation 14), common traits of large flowing conduits. In case of an extremely dry soil (large pressure head value), a low initial hydraulic conductivity value is obtained when close to dry conditions ($S_e \approx 0$) according to Equation 3. From the numerical solution point of view, no inflow will occur unless a large head gradient is induced between the boundary and the domain. This numerical effect was also pointed out by Wang and Narasimhan (1993). In addition, they pointed that Equation 14 has a limited range of validity if estimated from capillary theory. This is because

the radius of the meniscus inside the parallel plates will tend to infinity for very wide fractures which result in no capillary rise at all. Based on a value of $\tau = 7.28 \times 10^{-2}$ N/m for water at 20°C, the capillary rise relation cannot be used for fractures with apertures b>3.83 mm. If used, the maximum possible value of α when using Equation 14 is 255.9 1/m. For this study we will refer to this value as α_{max}.

In order to improve the method for defining the α coefficient for fast infiltration processes, we propose to replace Equation 14 with the $\alpha_{1\%}$ presented in Equation 15 so that the residual water content is maintained for a pressure head close to h_{ini} inside the fracture. This is achieved by setting the initial specific water content inside the fracture equal to 1%. Hence, the updated α parameter value can be calculated from Equation 2 as

$$\alpha_{1\%} = \frac{(S_e(h_{ini})^{1/m} - 1)^{1/n}}{h_{ini}} \quad S_e(h_{ini}) = 1\% \tag{15}$$

In this manner, any slight increase in pressure head in the upper boundary will immediately result in instantaneous infiltration. This is more similar to the observed physical behavior of a fracture under ponding conditions, with no entrapped air resistance. Note that Equations 14 and 15 are both used to define the SWRC and hydraulic conductivity function (Equations 2 and 3) for both EM and DPM fracture subsystems in all the simulations.

3.2.3. Fracture SWRC Exponent *n*

The exponent n from Equation 2 is commonly fixed to values close to 1 for impermeable soils like clays. For coarser soils like sands, n is fixed to values close to 2.5 and above (Carsel & Parrish, 1988; Vogel, van Genuchten, & Cislerova, 2000). We chose an exponent n equal to 4 as an initial estimate for the fitting of the SWRC of fracture subsystem. This represents the behavior of a highly permeable continuum which will saturate fast.

3.3. Interface Hydraulic Conductivity Function K_a

As a first approximation of K_a, we averaged the hydraulic conductivities from both fracture and matrix. Hence, the K_a can be written as

$$K_{a_{ave}} = \frac{K_m(h_m) + K_f(h_f)}{2} \tag{16}$$

Originally, Gerke and van Genuchten (1993b) proposed an approximation for the interface hydraulic conductivity K_a based on the arithmetic mean of the matrix hydraulic conductivity evaluated at the pressure head values of matrix and fracture domains. This approach was selected as it takes into account the local distribution of pressure heads in the matrix domain for calculating the exchange flux. The distribution of horizontal local pressure heads in the small fracture domain was not thought to be relevant because the lower conductive matrix domain was mainly controlling the local exchange. Because of this, K_a was written as

$$K_{a_{ari}} = \frac{K_m(h_m) + K_m(h_f)}{2} \tag{17}$$

Ray et al. (2004) suggested that the interface can be partly obstructed by the buildup of organic matter coatings and therefore the interface hydraulic conductivity function could be more similar to a fraction of the local hydraulic conductivity but evaluated based on the lowest of relative conductivity values between k_{r_m} and k_{r_f}. We tested this function as well, but we needed to take into account that the permeability of the fracture domain is significantly larger than the one of the clay matrix. Hence, we modified it by multiplying K_m by a factor λ larger than 1. This will ensure that the hydraulic conductivity value of the exchange function will always be larger than the one used locally for the matrix. Still, this function may be used for fractured soils with coatings as well by fixing λ to values lower than 1. For our case, the function is written as

$$K_{a_\lambda} = \min\{k_{r_f}(h_f),\ k_{r_m}(h_m)\}(K_{s_m}\lambda) \tag{18}$$

Experimental results presented by Song et al. (2018) showed that the saturated hydraulic conductivity at the interface between fractures and clay may be 1 order of magnitude larger than the one of the K_{s_m} which will represent a value of $\lambda = 10$ on 18.

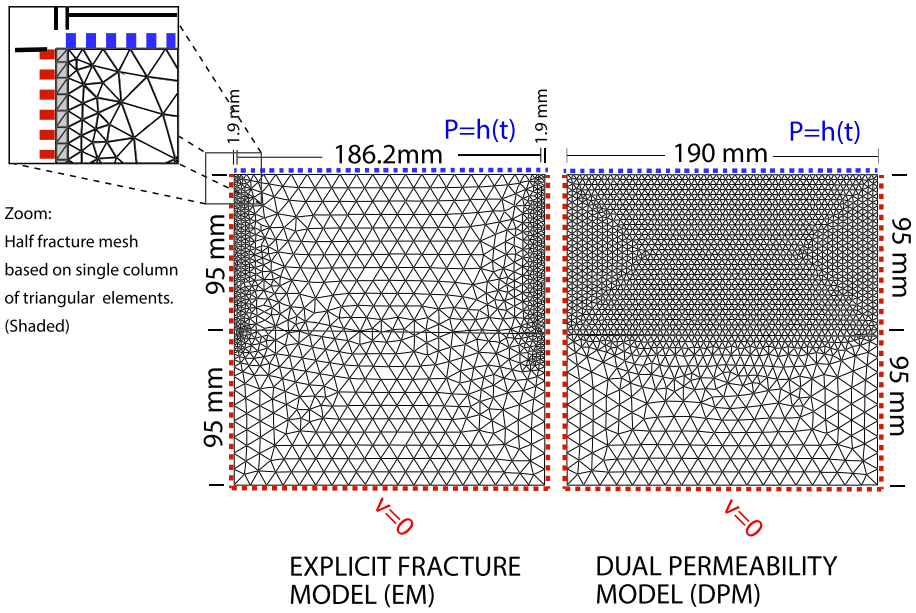

Figure 2. Dimensions, boundary conditions, and FEM mesh of EM and DPM.

The K_a function was reformulated by Gerke et al. (2013) by choosing the lowest hydraulic conductivity value obtained from both subsystems SWRC but evaluated in the largest pressure head value from both subsystems at the same location. This formulation will represent that the flow occurs from the highest head toward the lowest head but regulated by the less permeable of the subsystems in that instant of time. The K_a function was written as

$$K_{a_{min}} = \min\{K_m(h_f),\, K_f(h_f)\} \quad h_f \geq h_m \tag{19}$$

$$K_{a_{min}} = \min\{K_m(h_m),\, K_f(h_m)\} \quad h_f < h_m \tag{20}$$

From all four previously explained K_a approximations, only the one presented in Equation 17 has been evaluated in terms of its performance with respect to its equivalent EM in 1-D (Gerke & van Genuchten, 1993b). In our study we tested all three different K_a approximations so that we can recommend the best performing in the case of fractured clays.

4. Numerical Model

4.1. Domain Definition and Boundary Conditions

Both EM and DPM numerical models are implemented in a finite element solver for Richard's equation as part of the COMSOL multiphysics software (Comsol, 2018). The implementation of the DPM is based on the method presented by Shao et al. (2015). Both EM and DPM were defined as two square soil domains of $0.19 \times 0.19\ m^2$ divided into two layers for all numerical experiments: the upper one in which fractures and clay are present and a lower one in which only clay is present. The initial pressure head (h_{ini}) is set to -3.3m for all domains in each experiment. This is a common value for field capacity (h_{fc}) of clayey soils. As a testing feature, both models (EM and DPM) were conceptualized as "buckets." This means that there is no possible outflow from the lateral or bottom boundaries (dashed red lines in Figure 2). This configuration allows to reach full saturation at a certain point in time of the simulation for both fracture and matrix domains. We acknowledge that numerical stability, meshing strategies, and accuracy of the model are also very important when proposing a numerical model, but for the present study we only aim to answer the question whether it is possible to represent the fracture clay problem conceptualized as a DPM (bench marking it with an EM) rather than proposing the most efficient and robust numerical approach to solve it.

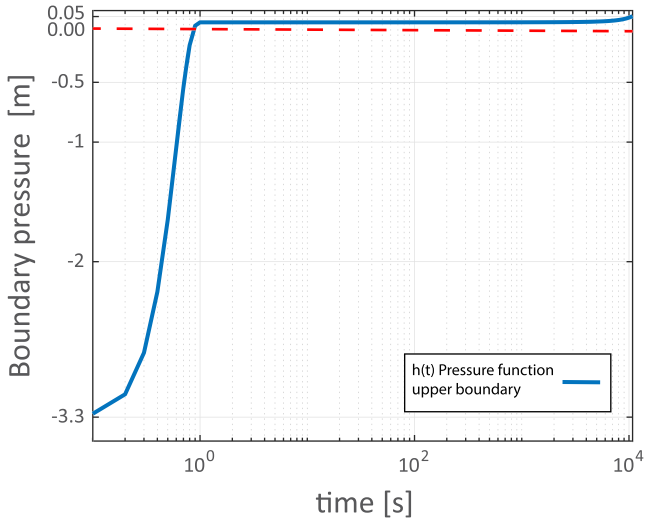

Figure 3. Upper boundary pressure as a function of time for both EM and DPM. Both axes are plotted in log scale.

For the upper boundary condition of both models, a transient pressure head boundary condition (Dirichlet) was defined. It was set to simulate a time-dependent ponding event (dashed blue lines in Figure 2). This allowed to simplify the model as it is common practice, to use a combined type of boundary condition (Dirichlet and Neumann) for representing rainfall-driven infiltration processes (Chui & Freyberg, 2009). The condition was designed by implementing a sharp jump in the first second of the simulation going from −3.3 m, which corresponds to the initial pressure head, to 0 m (see Figure 3). This ensures that inflow starts as soon as the boundary pressure value becomes positive. For the rest of the 3 hr of simulation, the water level rises until it reaches +0.05 m.

For the EM bucket, one fracture is explicitly represented as two separate halves on the upper layer located at each side (Gerke & van Genuchten, 1993a). In this way, the contribution of water between domains comes from both sides of the fracture. For this study, the fracture has an average aperture of $b = 3.8$ mm spaced at $a = 186.2$ mm. These values correspond to a $n_c = 0.02$ for the upper layer in both lateral and top areal projections. The second bucket presented in Figure 2) corresponds to the equivalent DPM REA of the first one. Note that the size of the domains is the same for both EM and DPM and the volumetric scaling of the DPM is adjusted by the inclusion of w_f and w_m in Equations 9 and 10.

4.2. Experiments

Experiment 1: SWRC α parameter. This experiment was developed to compare the performance of two EM REAs (left side block of Figure 2) while using α_{max} and $\alpha_{1\%}$ as parameter fittings for the fracture domain. For comparison, a DPM REA is simulated with $\alpha_{1\%}$ as α parameter for the fracture domain as well. This allowed to see how the fracture reacts to a small change in the pressure head and how much faster is the infiltration process.

Experiment 2: Interface hydraulic conductivity function. This experiment was developed to estimate the difference in the mass exchange between fracture and matrix derived using the four K_a functions presented in section 3.2. In these simulations we also tested the influence of the scaling coefficient γ in the different K_a functions, changing its value from 0.4 to 1.0. This modification was done as a sensitivity exercise, because the value obtained by Gerke and van Genuchten (1993b) was calibrated for a $K_{a_{ari}}$ only.

Experiment 3: SWRC exponent. For coarse-textured soils, exponents tend to be larger than 2, whereas for fine-textured soils, they are closer to 1.2 (Carsel & Parrish, 1988). In this experiment we wanted to quantify the influence of the exponent n in the DPM model in terms of infiltration rates and mass exchange.

Several parameters for the characterization of the domains and exchange functions were set constant throughout all the three experiments for both EM and DPM and are presented in Table 1.

A summary of the experiments parameter variations is presented in Table 2.

5. Results

For each of the experiments, all modifications were evaluated by simulations that represented 3 hr time span with variable time stepping depending on the moment of simulation (e.g., time steps of 0.05 s during fracture filling and between 0.5 and 30 s during matrix saturation). All simulations where evaluated based on their accumulated upper boundary infiltration, their accumulated mass exchange, and their REA average moisture content in time, all for both fracture and matrix subsystems.

5.1. Experiment 1

The first observation we want to point out from Simulation 1.1 is that the total infiltrated volume trough the fracture domain at the end of the simulation (I_f) is 1×10^{-16} m^2. This order of magnitude is negligible even when compared to the initial infiltrated volume during the first 0.0001 s through the matrix subsystem, which is around 1×10^{-10} m^2. It is also negligible when compared to the initial infiltrated volumes through

Table 1
Constant Values of Parameters of EM and DPM for All Simulations

Parameter	Unit	Value
w_f	—	0.02
w_m	—	0.98
β	—	3
h_{ini}	m	-3.3 (h_{fc})
a	mm	3.8
b	mm	186.2
φ	(°)	0
$K_{s_f} = K_3$ (fracture)	m/s	11.75
K_{s_m} (clay)	m/s	2.65×10^{-6}
α (clay)	1/m	2.4
α_{max} (fracture)[a]	1/m	255.9
$\alpha_{1\%}$ (fracture)	1/m	1.406
n (clay)	—	1.5
θ_s (clay)	m^2/m^2	0.43
θ_r (clay)	m^2/m^2	0.086
θ_s (fracture)	m^2/m^2	0.99
θ_r (fracture)	m^2/m^2	0.01

[a]Used only in Simulation 1.1 (EM).

the fracture of Simulations 1.2 and 1.3 (1×10^{-8} m^2). Therefore, the coarse black dashed line that should correspond to I_f (Figure 4a) for the results of Simulation 1.1 was not included.

This result was expected as the α_{max} will impose a very low hydraulic conductivity value (1×10^{-27} m/s) inside the fracture which will result in a very steep wetting front. In addition, the initial conditions we defined for the model induce capillary pressure head gradients that dominate the gravity gradients by far. For the ponding condition, the influx at the inlet depends on the averaging between the fracture-saturated hydraulic conductivity imposed along the boundary and the hydraulic conductivity inside the fracture. This averaging often results in underestimation or overestimation of the flux. In the present case this error induced almost all the influx to ingress the system only trough the matrix boundary. This problem may be solved by a mesh refinement procedure, but improving the EM model with α_{max} is useless for our study and out of the scope.

Regarding Simulations 1.2 and 1.3 where α parameter was set equal to $\alpha_{1\%}$, their initial response inside the fracture to the sharp increase in pressure is instantaneous. The main observed difference between these two subsystem responses is that the EM finishes with a larger infiltrated volume at the end of the simulation. For the infiltration through the matrix upper boundary I_m (Figure 4b), the EM with α_{max} (Simulation 1.1) of total infiltrated volume is almost the same as for Simulations 1.2 and 1.3. This is contrary to the estimated infiltration of the DPM with $\alpha_{1\%}$ for which most of the inflow to the REA happened through the fracture domain. From this plot it can already be implied that the mass exchange is too large, and therefore most of the water that saturates the REA has entered through the fracture domain. Another interesting result from the simulation with α_{max} is that despite representing a wrong physical parameterization of the system, it can result in a good estimation of the total infiltrated amount of water of the complete system in the long term (see dashed lines in I_f+I_m Figure 4c).

The changes in water content in time for each subsystem are presented in Figure 5. For the fracture domain (Figure 5a), Simulation 1.1 remains dry during the entire simulation time, whereas Simulations 1.2 and 1.3 saturate in less than a second. Note that as soon as there is a pressure gradient in the boundary of the fracture, disregarding if the boundary load is still negative, inflow occurs. This is the reason why both EM and DPM with $\alpha_{1\%}$ "fill" in less than 1 s which is the time it takes for the loading function to reach values greater

Table 2
Description and Values Used for the Different Simulations Used in Each of the Experiments

Simulation	Modification description	α_f	n_f	K_a	γ_w
1.1	SWRC α parameter based on capillary rise (Equation 14) in EM	α_{max}	4	—	0.4
1.2a	SWRC α parameter (Equation 15) in EM (reference)	$\alpha_{1\%}$	4	—	0.4
1.3	SWRC α parameter (Equation 15) in DPM	$\alpha_{1\%}$	4	$K_{a_{ari}}$	0.4
2.1	K_a based on average function (Equation 16) in DPM	$\alpha_{1\%}$	4	$K_{a_{ave}}$	0.4
2.2b	K_a based on average function (Equation 17) in DPM	$\alpha_{1\%}$	4	$K_{a_{ari}}$	0.4
2.3	K_a based on lambda function (Equation 18) with $\lambda = 10$ in DPM	$\alpha_{1\%}$	4	K_{a_λ}	0.4
2.4	K_a based on lambda function (Equation 18) with $\lambda = 10$ in DPM	$\alpha_{1\%}$	4	K_{a_λ}	1.0
2.5	K_a based on minimum function (Equations 19 and 20) in DPM	$\alpha_{1\%}$	4	$K_{a_{min}}$	0.4
2.6	K_a based on minimum function (Equations 19 and 20) in DPM	$\alpha_{1\%}$	4	$K_{a_{min}}$	1.0
3.1	Sand exponent n of the fracture SWRC	$\alpha_{1\%}$	2.68	$K_{a_{min}}$	0.4
3.2	Coarser sand exponent n of the fracture SWRC	$\alpha_{1\%}$	3	$K_{a_{min}}$	0.4
3.3c	Exponent n of the fracture SWRC used in the EM Reference model	$\alpha_{1\%}$	4	$K_{a_{min}}$	0.4
3.4	Large exponent n of the fracture SWRC	$\alpha_{1\%}$	5	$K_{a_{min}}$	0.4
3.5	Larger exponent n of the fracture SWRC	$\alpha_{1\%}$	6	$K_{a_{min}}$	0.4
FINAL	Final calibration based on the three experiments	$\alpha_{1\%}$	4	$K_{a_{min}}$	0.05

Note. Subscript $_f$ is for values used in the SWRC of the fracture.
[a]Reference EM model to compare with other DPM models. [b]Same simulation as 1.3. [c]Same simulation as 2.5.

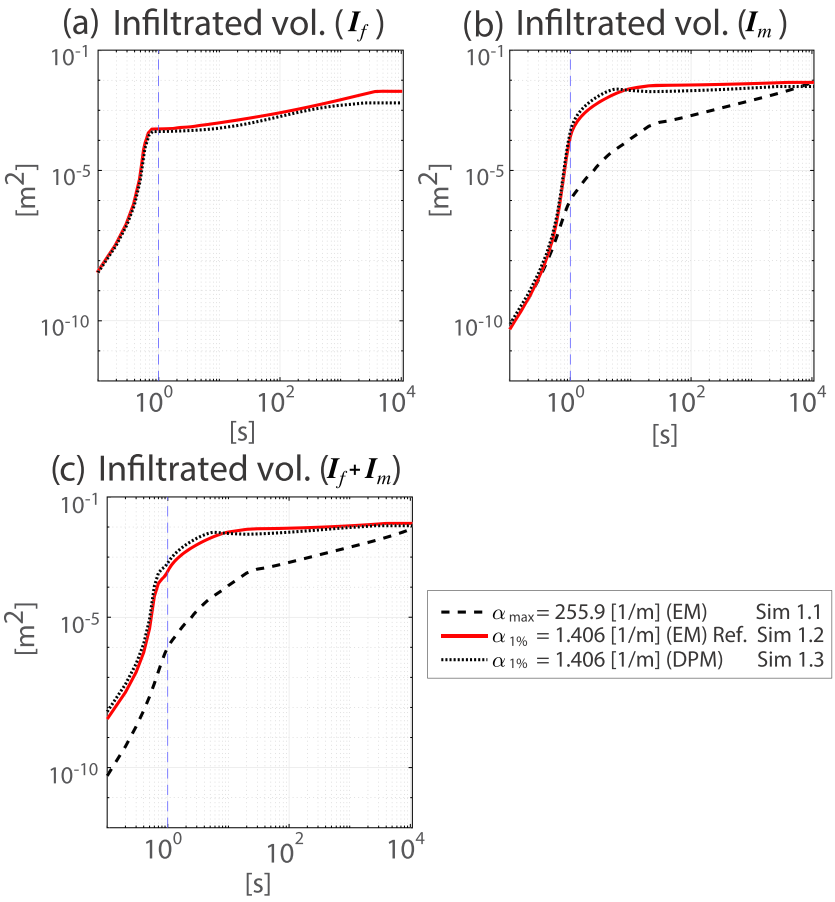

Figure 4. Results of the cumulative infiltrated volume in time from the upper boundary in (a) the fracture (I_f), (b) the matrix (I_m), and (c) the complete system (I_f+I_m).

than 0 (see Figure 3). The moisture content is also influenced by the exchange between fracture and matrix and vice versa, and the results show that on average the DPM simulation $\alpha_{1\%}$ reaches full saturation faster than the reference model. This indicates that the exchange term "hydraulic conductivity" or the other scaling parameters result in a faster mass exchange between fracture and matrix domains. In addition, it can also be observed how the matrix of the EM with α_{max} takes significantly more time to saturate despite always having greater infiltration rates (estimated as the slope of the accumulated infiltration I_m in Figure 5b, with respect to the other two simulations.

The average exchange flux and its integral (volume) in time are presented in Figures 6a and 6b. At a first glance it is noticed that the mass exchange of the EM with α_{max} is not plotted in both figures as almost no water infiltrated the fracture. Nevertheless, in an ideal fracture representation it can also happen that the pressure inside the matrix at full saturation generates fluxes toward the inside of the fracture through the walls. This is not possible for the EM with α_{max}, as the initial hydraulic conductivity inside the fracture is very low so water cannot flow outside either. For the other two simulations, the initial exchange flux at first is significantly larger in the first 2 s in the reference simulation, but later, the DPM simulation becomes larger for the rest of the simulation. This results in a faster saturation of the reference model during the first 10 s.

A second observation is that the EM $\alpha_{1\%}$ shows some negative exchange (matrix to fracture) between 2 and 5 s (plotted with lighter color as EM). This does not happen in the DPM model which is an additional reason for the DPM to saturate faster. Note that for the average exchange (Figure 6a), the time span of exchange is also shorter as a result of the faster saturation process. It is expected that this negative exchange is originated because the hydraulic conductivity on the interface is highly influenced by the large value inside the

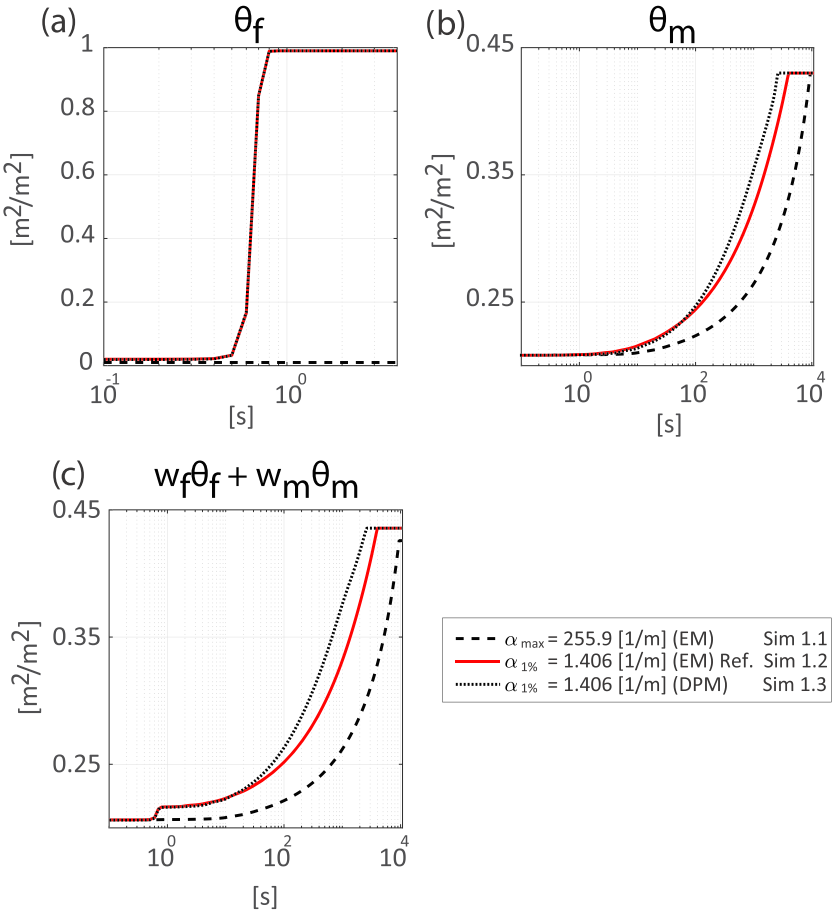

Figure 5. Experiment 1 results. Average water content in (a) the fracture, (b) the matrix, and the (c) complete system. The θ_f presented in panel a is only plotted for the first 2 s as it reaches saturation faster than the matrix (θ_m).

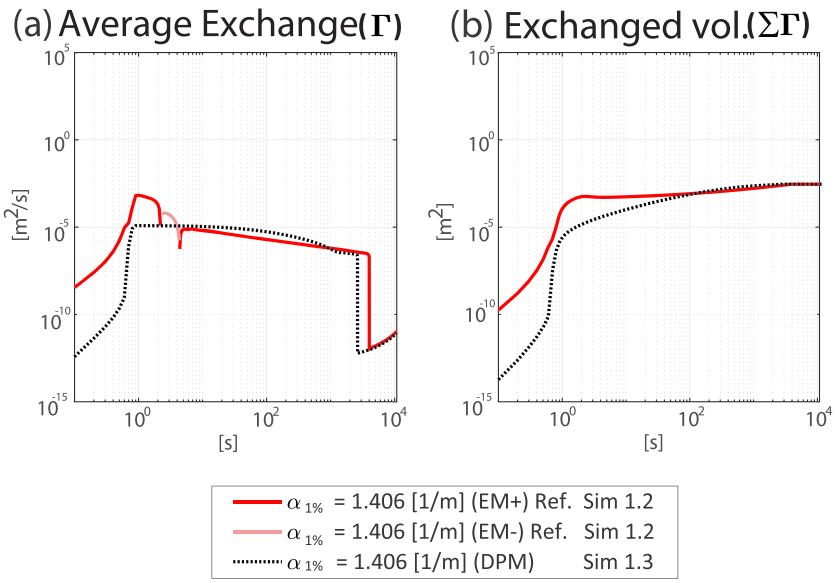

Figure 6. Experiment 1 results. (a) Average exchange rate and (b) accumulated exchanged volume in time from fracture to matrix (+) in the EM (red line). The (−) represents the exchange from matrix to fracture in the EM (pink line). The exchange in the DPM is always (+) from fracture to matrix (black dashed line).

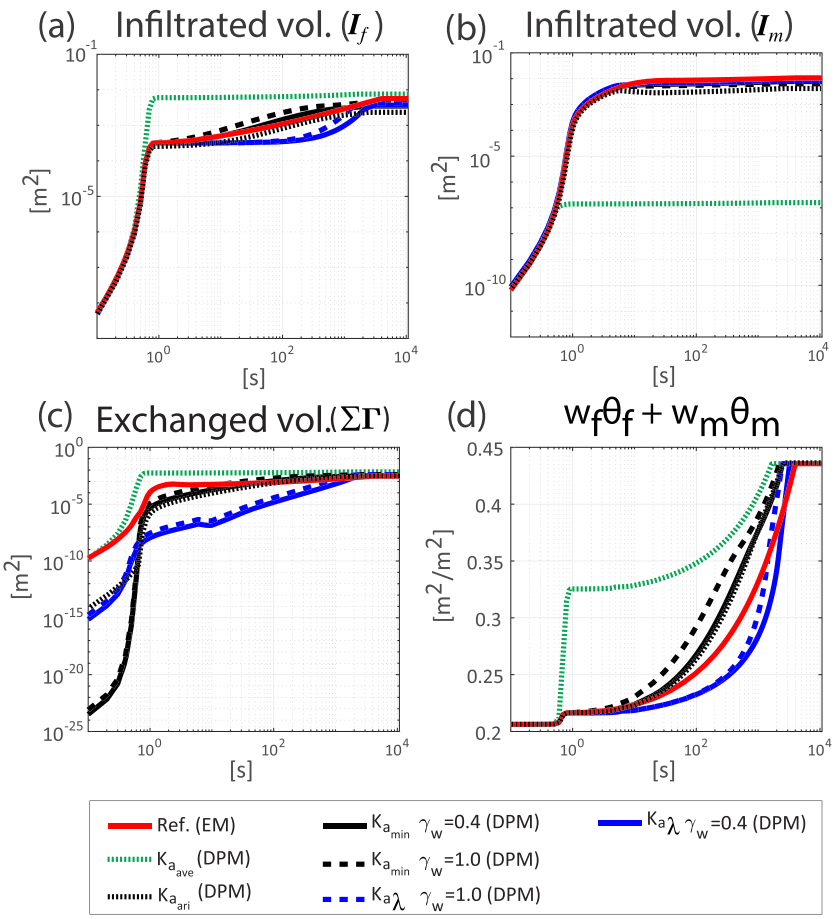

Figure 7. Experiment 2 results. Infiltrated volumes (a and b), exchanged volumes (c), and water content for different mass exchange functions (d) for different K_a functions.

fracture, which also represents too little resistance to flow, but because of the fast saturation along the matrix domain, the biggest head difference is found in the matrix domain. This will result in influx from matrix to fracture. To prove this assumption, three model runs with the same configuration but different meshing sizes where tested, and all of them presented the same negative exchange but with slightly different values. This same exercise was repeated but with K_{sf} lower than K_3, and the result presented no negative exchange.

5.2. Experiment 2

In this experiment, two additional tests for the simulations of $K_{a_{min}}$ and K_{a_λ} were included to test the influence of the γ_w factor. Note that the coefficient estimated by Gerke and van Genuchten (1993b) is calibrated for the $K_{a_{ari}}$ function only. This is shown in Figures 7a and 7b where the infiltrated volumes through the upper boundary of the fracture I_f and the matrix I_m are presented for each interface K_a tested function.

In Figures 7c and 7d, the accumulated exchange and the average water content in time of the complete REA are also presented. From the three different K_a functions, the $K_{a_{ave}}$ is the only one that overestimates the total infiltrated volume.

For the two cases of $K_{a_{min}}$, they simulate the total infiltrated volume in the fracture compared to the EM reference model. In here, a slight overestimation between the 2 and 1,000 s period can be observed. Yet, this is the one that agrees the most with respect to the EM in terms of the total infiltrated volume. For K_{a_λ} DPM, it first underestimates the total infiltrated volume, and then by 3,000 s it increases significantly surpassing the infiltrated volume in the EM. Still, both simulations reach almost the same total infiltrated volume 3.5×10^{-3} m^2

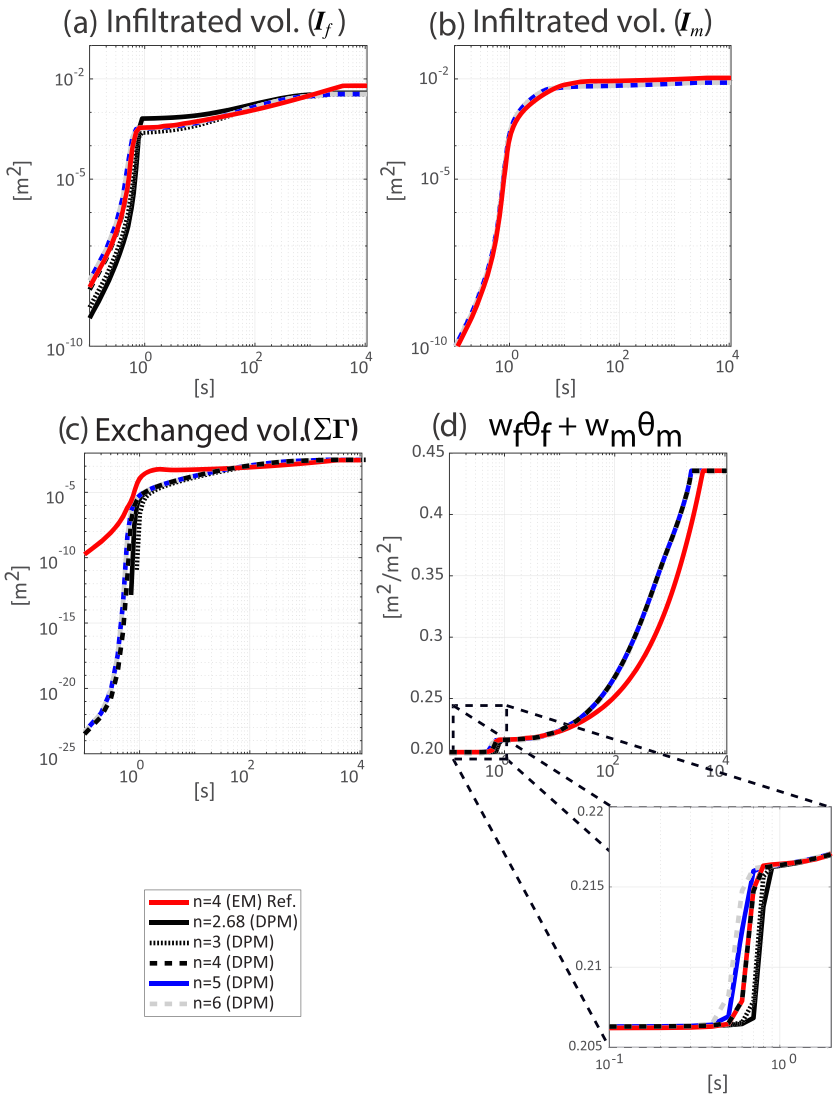

Figure 8. Experiment 3 results. (a, b) Infiltrated volumes, (c) exchanged volumes, and (d) water content for different exponents (n).

when compared to the reference EM model. From all simulations, $K_{a_{ari}}$ performs the best for the first 1,000 s but underestimates the total infiltration through the fracture. With respect to the infiltration through the matrix, the reference and the DPM's with $K_{a_{ari}}$, $K_{a_{min}}$, and K_{a_λ} result in very similar trends and total infiltrated volumes in time. The only DPM modification that underestimates the infiltration is $K_{a_{ave}}$.

For the exchange of mass between fracture and matrix, the $K_{a_{ave}}$ DPM model starts with the same initial exchanged volume as the EM reference, but before the first second of infiltration has passed, it has already exchanged more than 80% of the the total volume by the reference model. Note that for this experiment, α_{max} is used, so infiltration also happens very fast. The excess of exchange is derived from estimating K_a directly from the K_3 as it is orders of magnitude larger than the one used for K_m.

From the other two models, large discrepancy in the initial exchange during the fracture filling is observed. $K_{a_{min}}$ recovers fast after approximately 2 min even surpassing the exchanged volume of the EM. This also happens to the $K_{a_{ari}}$ but with a lower rate. A larger exchange will always imply that the REA will reach saturation faster, which happens to all K_a functions in the long run. While $K_{a_{min}}$, $K_{a_{ari}}$, and K_{a_λ} present relatively better results than the K_a functions, we suspect that calibrating the exchange will be easier for the $K_{a_{min}}$, as the trend is more similar to the EM (small dashed black line I_f in Figure 7a). This is not the case for the K_{a_λ}

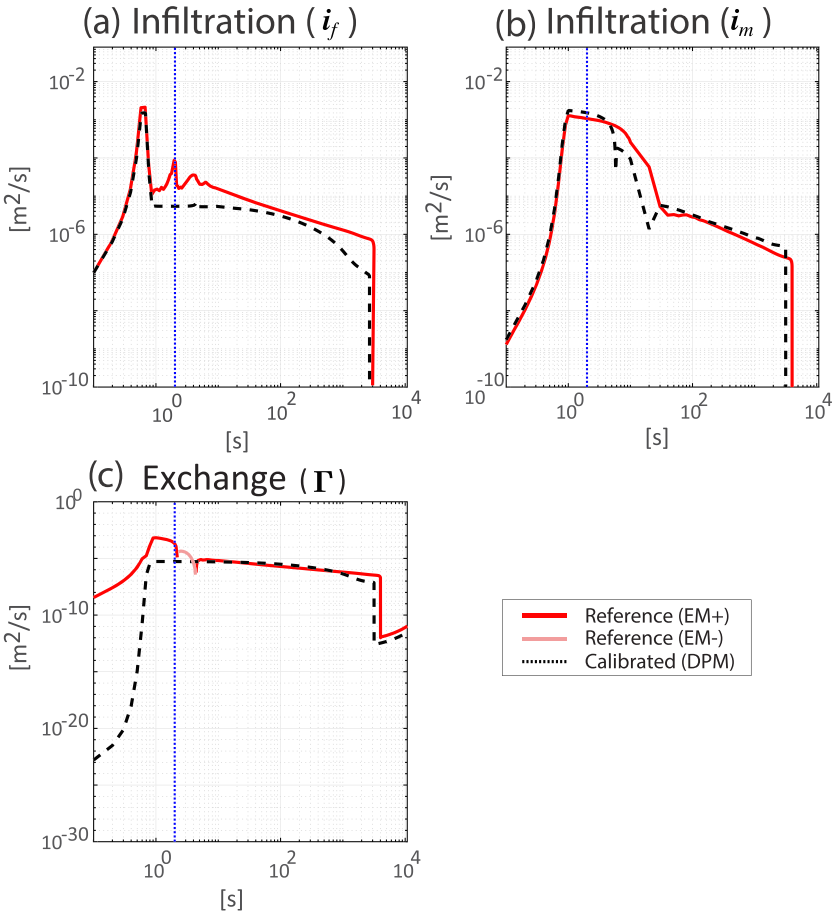

Figure 9. (a, b) Infiltration and (c) exchanged fluxes for calibrated model. Blue vertical dashed line defines the first second in which full saturation of the fracture domains occurs.

DPM (dashed blue line in Figure 7a) for which concave and convex features are observed in infiltration volumes and mass exchange curves. For this reasons and because the K_{a_λ} has the additional λ parameter to calibrate, $K_{a_{min}}$ is chosen as the better performing among all. $K_{a_{ari}}$ is the second best performer of the group with a slightly better performance on the water content change in time (black fine dashed line in Figure 7d).

5.3. Experiment 3

In Experiment 3, the $K_{a_{min}}$ function with an scaling coefficient $\gamma = 0.4$ was used as a benchmark for all simulations. The results from the different simulations and model features using different n' exponents are presented in Figure 8.

In terms of fracture infiltration (Figure 8a), it is shown that values of $n<4$ deviate along the complete filling and exchange process, while values $n \geq 4$ perform better. Yet, all of n tested values result in later full saturation of the system with respect to the EM. Also, the variation among experiments of the n value of the fracture domain had no significant influence in the total infiltrated volume over the matrix inflow I_m (Figure 8b) in any of the simulations. Regarding the total exchanged volumes (Figure 8c), they do tend to be different among all DPMs before the 2,000 s time threshold, but later on, they become almost equal to the EM until the end of the simulations. It is also observed how lower values of the n exponent result in larger initial exchanged volumes (Figure 8c) which are mostly triggered at the end of the filling period ($t<1$ s).

For the water content (Figure 8d), values of $n>4$ gave slightly better results in the long term and are found in literature for very permeable soils like coarse sands. Yet, $n = 4$ performs better during the fracture filling period (dashed black line in the zoom of Figure 8d). Afterward it starts deviating, resulting in a faster saturation

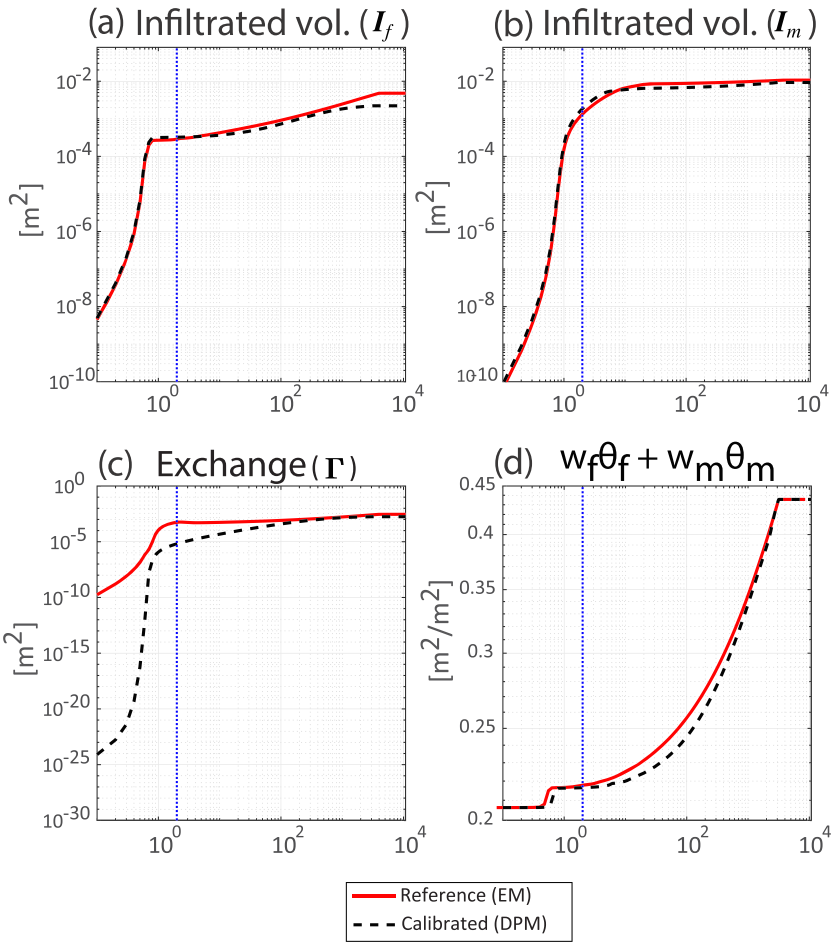

Figure 10. (a, b) Infiltrated volumes, (c) exchanged volumes, and (d) water content for calibrated model. Blue vertical dashed line defines the first second in which full saturation of the fracture domains occurs.

time of the REA with respect to the reference. Still, the results show generally that there is no significant influence or improvement in performance with respect to the EM when varying the value of the n exponent.

5.4. Final Calibrated Model

Based on the results obtained in the three experiments, it was decided that the optimal configuration was obtained by assuming the following:

1. a water entry coefficient equal to $\alpha_{1\%}$ (Equation 10);
2. a K_{s_f} equal to K_3 (Equation 13);
3. a K_a function for Γ of the type $K_{a_{min}}$ (Equations 18 and 19);
4. a $\gamma_w = 0.05$, obtained from calibration;
5. a SWRC exponent $n = 4$ chosen arbitrarily since the start.

The performance of the calibrated DPM inflow rates and mass exchange rates in time are presented in Figure 9. The modification of the DPM model fairly reproduces the main features of the infiltration of both fracture and matrix. Furthermore, the exchange rates are quite similar after the negative exchange period.

The saturation moment is another feature which can be determined as the time both i_f and i_m plots end in a sharp bend downward. This sharp change means that no more water is infiltrating the system. The DPM model is also capable of reproducing the moment for which water reaches the end tip of the fracture which is characterized by the fast change in infiltration (Peak on 0.7 s; Figure 9a). The infiltration fluxes in the matrix (Figure 9b) give a similar picture but with a smoother bend. Note that the upper mass infiltration

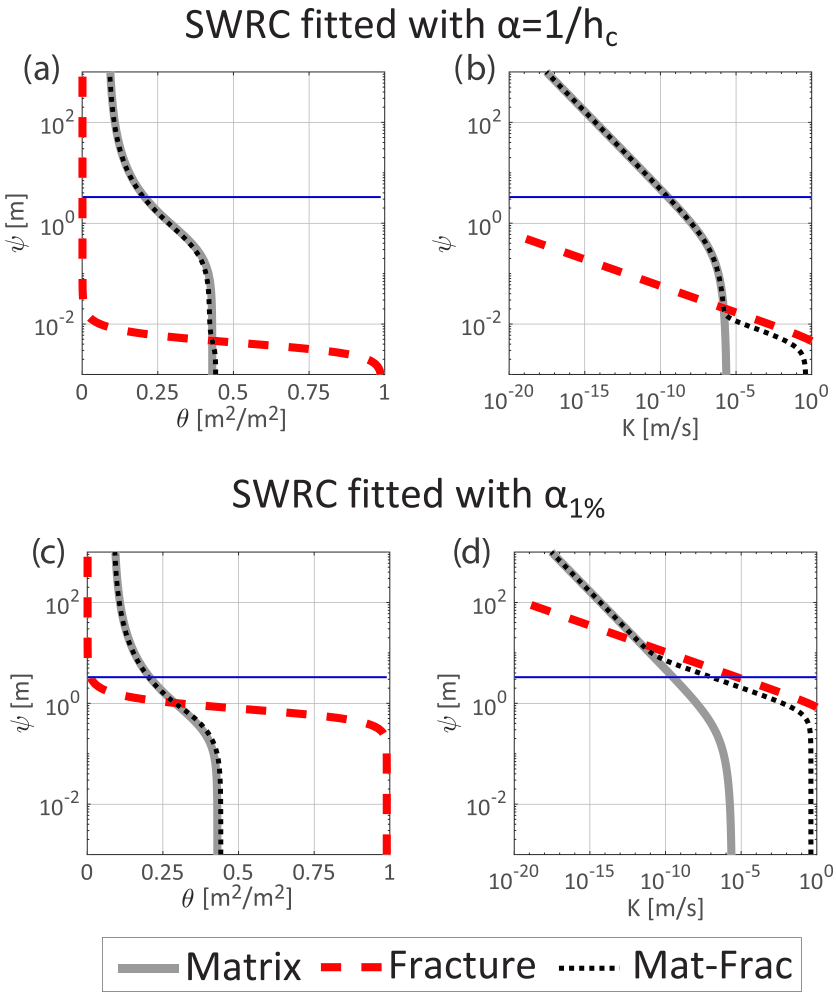

Figure 11. Comparison of SWRCs fitted with $\alpha = 1/h_c$ and $\alpha_{1\%}$. The blue horizontal line represents the initial pressure head value. Soil water retention curve and hydraulic conductivity functions fitted with α_{max} (a, b) and fitted with α1% (c, d).

of the matrix is regulated not only by the SWRC but by the exchange with the fracture as well. As soon as the fracture starts to saturate, the head difference between both domains reduces and so does the mass exchange flux. The volumes or integral of the fluxes from the calibrated model also show a good performance in general and are presented in Figure 10.

The whole experiment was calibrated by trying to achieve the same total saturation time (4,020 s in Figure 10d). The calibration obtained reaches saturation in 3,810 s, equivalent to an error of 5.2%. In these results we can see that the infiltrated total volume through the fracture is smaller than the one of the reference. This is the result from having larger mass exchange since the start of the simulation. Yet the filling and saturation time are quite similar between the DPM and EM as well as the final exchanged volumes.

6. Discussion

6.1. Fracture Filling

For the specific case of the Mualem-van Genuchten closed form equation, it is often misunderstood that the α coefficient is related to the inverse of the capillary rise at which the largest pore starts draining its water as in the case of the Brooks-Corey water retention model. Note that most literature that presents SWRC values (Carsel & Parrish, 1988; Ghanbarian-Alavijeh et al., 2010; Tinjum et al., 1997; Vogel, van Genuchten, and Cislerova 2000) show that small α values fit best for low permeability soils. However, this assumption is

not true as the α parameter in the Mualem-van Genuchten model corresponds to a purely numerical fitting parameter which cannot be inferred from the physical behavior of the soil like the capillary rise, for example (Morel-Seytoux et al., 1996). In reality, this parameter rather reflects the response of the complete soil system (e.g., pore orientation, tortuosity, and connectivity). This is the main reason why there is no conceptual mistake on attributing a small α value to a highly permeable soil (fracture in our case) as the one obtained from using the $\alpha_{1\%}$ is purely an adaptation strategy for the fracture domain. The reason we decided to do this is that low α values shift the SWRC of the fracture upward (Figure 11a vs. 11c) which results in a greater value of the initial hydraulic conductivity inside the fracture, plus lower pressure head gradients will already induce large fluxes.

In Figure 11d, for example, it is close to 1×10^{-5} m/s where it crosses the blue line. Such a large value of hydraulic conductivity means that a small increase in top boundary head will immediately allow water to start flowing inside the fracture.

In this study we chose an initial specific water content equal to 1% arbitrarily. If a smaller value was chosen, it is expected that both DPM and EM infiltration will be equally affected. Specifically during the filling phase both models behave almost identically. This is not the case for the mass exchange, as a wetter boundary will increase the exchange for both models but in different orders of magnitude depending on which K_a function is chosen. Another arbitrary choice for this study was the rapid initial increase in head over the upper boundary condition (see Figure 3). This was set to change from a value of −3.3 to 0 m in 1 s. This choice was taken for two main reasons. The first one was the expected order of magnitude in terms of filling time when assuming no air resistance was present inside the fracture. The second one was that the smaller this value is chosen, the harder it is to achieve numerical convergence. This order of magnitude is proven to be solvable, and the results even showed that full saturation of the fracture occurs in less than 0.7 s under this boundary condition. Hence, the present model will also allow to calibrate the fracture response either by the initial filling boundary condition function (first second of this study) or by prescribed value of the saturated hydraulic conductivity of the fracture domain. The fracture filling should also be tested under drainage condition. This test becomes important as water stored in the fracture will eventually flow toward the matrix or from the matrix toward the fracture depending on the initial saturation of the fracture. This can also be tested under the assumption of $\alpha_{1\%}$ allowing a less restrictive infiltration.

Regarding the fracture infiltration, it is important to note that we are trying to approximate a fluid movement problem from a porous media modeling solution. One of the implications of such approximation is that the fracture will saturate from top to bottom. However, the resistance of air makes the fracture to fill in a lateral film that flow toward the bottom accumulating from bottom to top. While this can be a discrepancy with respect to water exchange measured in physical experiments, it is also important to note that DPM is an approximation to the EM for which the filling process is also from top to bottom. Furthermore, the presence of large pores may even represent an influx barrier as air cannot be displaced. This type of behavior is not represented by the actual calibration of the model, but it may be represented by fine tuning the $\alpha_{1\%}$ value to the one expected (or measured) when including the air resistance effect in the infiltration rate.

It is also important to point out that we intentionally defined the equation $\alpha_{1\%}$ in terms of h_{ini} instead of h_{fc}. The reason behind this choice was to allow the model to not only simulate very dry matrix and fracture initial conditions but to also simulate cases of an initial moist matrix in combination with very dry fractures. Note that the initial pressure head value of the matrix domain is also used as initial pressure head value for the fracture domain. If so, for an initial moist matrix, h_{ini} is required to be greater than h_{fc} of the soil. If the SWRC $\alpha_{1\%}$ of the fracture was parameterized as a function of h_{fc} instead of h_{ini}, the initial moisture conditions inside the fracture will be far greater than the chosen 1%. For the present study we defined $h_{ini} = h_{fc}$ as our main interest was to investigate very dry initial conditions of both matrix and fracture.

As a final remark it is important to acknowledge that the modification of the DPM presented in this paper is only valid as long as the inner fluxes remain in the laminar regime inside both domains. The approximation of Poiseuille type of flow inside the fracture is what allows to solve the whole system as a Darcian porous media numerical solution. For this reason we checked the inflow maximum velocities in the upper boundary of the fracture where we expect to have the fastest flows in both EM and DPM. The correspondent flow velocities are 0.00782 and 0.1973 m/s with Reynolds numbers of 1,481 and 747, correspondingly, both below 2,300 which classifies them as laminar.

6.2. K_a and the Exchange Term Γ

The first remark about the DPM used in the present study is that it is an approximation of the explicit domain model (EM), and therefore there will be some conditions for which DPM will underperform. The fracture initial filling is a good example of this. While the DPM model tends to recover and reach similar values of infiltration and exchange in the long term, there are large discrepancies with respect to the EM in terms of the exchange. Such discrepancies may be attributed to the K_a function chosen for the exchange term Γ and its calibration. Note that in terms of saturation of the fracture, all models but the $K_{a_{ave}}$ result in almost identical behavior during the fracture filling period (see Figure 7a). Yet $K_{a_{ave}}$ is the only function that starts at the same exchange value.

The infiltration from the upper boundary to the matrix shows good results for all K_a besides $K_{a_{ave}}$. This shows the influence of the exchange calibration in the infiltration rates. The fast increase of moisture content in the first seconds is the result of such a fast exchange (green dashed line in Figure 7a). During this period larger head differences are expected to be exerted along the interface between fracture and matrix. These differences will result in larger mass exchanges. These differences do not necessarily imply that the arithmetic function is wrong. It only means that it was originally derived and calibrated for the condition in which the fracture domain was fully saturated since the start of the simulation and for closer saturated K_m and K_f values in terms of orders of magnitude. From the present study it was observed that the most optimal choice, in terms of the interface hydraulic conductivity function, is $K_{a_{min}}$. It proved to be the best approximation in terms of infiltration for both fracture and matrix. In terms of the exchange, it also proved that without any prior calibration of γ, the $K_{a_{min}}$ was able to rapidly reach the total infiltrated volume in the EM at 200 (see Figure 7d). The $\gamma_w = 0.4$ was calibrated originally for the arithmetic approximation by Gerke and van Genuchten (1993b). This result gives rise to the question of whether the original value should continue to be fixed as a constant or should be calibrated, specially for models in which the fractured domain is not fully saturated since the start. Note that Gerke and van Genuchten (1993b) also pointed out that it would be more correct to express the coefficient as a function of the head as $\gamma_w(h_m)$.

In this study, it was also observed that no matter the choice of mass exchange function (from the three studied), the model can only be calibrated to achieve either the same time of saturation or the same exchanged volume but not both in terms of γ and β. In case of calibration for the exchange (the present study calibrated the model to achieve the same time of saturation), it might be feasible to use the $K_{a_{ave}}$ but with a K_f value smaller than the one obtained for K_3 to avoid the excessive exchange during the fracture filling. As an initial guess, one could use the observation reported by Song et al. (2018) where K_a is around 10 times K_m.

Another possibility to improve the accuracy of the model may be to use $K_{a_{ave}}$ during the filling period and switch to $K_{a_{min}}$ in the later stage. In that way we ensure a fast inflow during the filling period resulting in a smaller exchange and an accurate saturation curve and time. All previous consideration leave room for further research regarding the exchange functions and how to better represent the hydraulic conductivity along the interface between fracture and matrix.

6.3. SWRC Exponent n

The results from the third experiment show that the exponent n, only has significant influence during the fracture filling period and that values above 5 will not increase the infiltration rates much further. Nevertheless, the exponent of the SWRC is required to calculate the $\alpha_{1\%}$. In this study, the exponent n was varied from 2.68, which corresponds to the one suggested by Carsel and Parrish (1988) for coarse sand, to 6, which we determined as an unrealistic value. The resulting α values from these n's were 4.7 and 0.76 1/m which are in a good order of magnitude in general terms with respect to what soils are fitted to.

While no major influence in the infiltration or total exchanged volume was observed when varying the SWRC n, it does have an influence in the numerical solution complexity. This exponent determines the slope of the SWRC of the fracture. Ideally, a fast responding domain should be represented as an almost horizontally flat line in the midsection of the SWRC so that subtle pressure gradients will immediately initiate inflow toward the fracture. However, flatter curves also represent more difficulty for the solver as smaller pressure gradients result in greater moisture variations. This means that on average, a larger number of iterations are required for the model to find the correct solution for every time step. Therefore, we recommend to use n values between 2.68 and 4 for calibration of single-macropore subsystems such as wide fractures. The

chosen value in this study aims to mimic the effective hydraulic conductivity behavior of a dual-permeability system rather than give the parameters a strict physical meaning.

7. Conclusions

In this paper we proposed a parameterization and mass exchange function for the original DPM proposed by Gerke and van Genuchten (1993a) for representing fractured clay in dry initial conditions. The modeling results showed good agreement between the explicit reference model and the DPM using the suggested parameterization and novel modified hydraulic function of fractures and interface mass exchange function. The recommended parameterization and model mass exchange function can be summarized as follows: (1) an α value equal to $\alpha_{1\%}$, (2) a hydraulic conductivity function for the interface set equal to $K_{a_{min}}$, (3) a K_{S_f} value equal or close to the one obtained from the "cubic law" (K_3), and (4) a SWRC exponent n fixed to 4. Setting the α parameter equal to $\alpha_{1\%}$ is a robust approach as it allows to simulate fast infiltration into cavities while using Richards equation solution. Moreover, the obtained values with this modification are in the range of previously reported values in literature for similar soils. The calibration was targeted to reach the same saturation time as the EM. It was also concluded that calibration can only be optimized with respect to the saturation time or to the total exchanged volume but not to both at the same time as the mass exchange term behaves differently during the filling time of the fracture. Regarding the mass exchange function, it was concluded that choosing $K_{a_{min}}$ gives better results with respect to the original $K_{a_{ari}}$ proposed by Gerke and van Genuchten (1993a). Furthermore, it was found that a value of 0.01 for the scaling coefficient γ_w gave the best fit with respect to the explicit equivalent model for representing a fractured clay. Hence, it was also concluded that setting the γ_w value equal to 0.4 as the original work from Gerke and van Genuchten (1993a) must be revised as this value was obtained for a finite set of particular numerical experiments in which the fractured domain started from a fully saturated moisture condition. Finally, it is also recommended to compare the performance of the proposed improvements to the original DPM presented in this paper against the results obtained from a Darcian matrix solution coupled to a Navier-Stokes fractured solution DPM as this one represents the most complex numerical solution to the fractured soil problem.

Acknowledgments

The authors acknowledge the European Commission (Horizon 2020) and the Netherlands Organisation for Scientific Research (NWO) for financial support within the Water JPI Call and the WaterWork2014 cofunded Call for project DOMINO ALWWW.2014.1. Data were not used nor created for this research.

References

Adam, N. K. (1930). *Physics and chemistry of surfaces*. Oxford: Oxford University Press.

Aguilar-López, J. P., Warmink, J. J., Schielen, R. M. J., & Hulscher, SJMH (2016). Piping erosion safety assessment of flood defences founded over sewer pipes. *European Journal of Environmental and Civil Engineering*, *22*(6), 707–735.

Barenblatt, G. I., Zheltov, I. P., & Kochina, I. N. (1960). Basic concepts in the theory of seepage of homogeneous liquids in fissured rocks [strata]. *Journal of Applied Mathematics and Mechanics*, *24*(5), 1286–1303.

Bear, J. (1972). *Dynamics of fluids in porous media*. New York: American Elsevier Pub. Co.

Beven, K. (2018). A century of denial: Preferential and nonequilibrium water flow in soils, 1864-1984. *Vadose Zone Journal*, *17*(1), 1–17.

Beven, K., & Germann, P. (2013). Macropores and water flow in soils revisited. *Water Resources Research*, *49*, 3071–3092. https://doi.org/10.1002/wrcr.20156

Brooks, R. H., & Corey, A. T. (1966). Properties of porous media affecting fluid flow. *Journal of the Irrigation and Drainage Division*, *92*(2), 61–90.

Carsel, R. F., & Parrish, R. S. (1988). Developing joint probability distributions of soil water retention characteristics. *Water Resources Research*, *24*(5), 755–769.

Celia, M. A., Bouloutas, E. T., & Zarba, R. L. (1990). A general mass-conservative numerical solution for the unsaturated flow equation. *Water Resources Research*, *26*(7), 1483–1496.

Chertkov, V. Y., & Ravina, I. (2001). Effect of interaggregate capillary cracks on the hydraulic conductivity of swelling clay soils. *Water Resources Research*, *37*(5), 1245–1256.

Chui, T. F. M., & Freyberg, D. L. (2009). Implementing hydrologic boundary conditions in a multiphysics model. *Journal of Hydrologic Engineering*, *14*(12), 1374–1377.

Comsol, I. (2018). *Comsol multiphysics reference manual, version 5.3a*. Burlington, MA: COMSOL, Inc.

Drumm, E., Boles, D., & Wilson, G. (1997). Desiccation cracks result in preferential flow. *Geotechnical News*, *15*(2), 22–25.

Dykhuizen, R. C. (1987). Transport of solutes through unsaturated fractured media. *Water Research*, *21*(12), 1531–1539.

Ebel, B. A., Mirus, B. B., Heppner, C. S., VanderKwaak, J. E., & Loague, K. (2009). First-order exchange coefficient coupling for simulating surface water–groundwater interactions: Parameter sensitivity and consistency with a physics-based approach. *Hydrological Processes*, *23*(13), 1949–1959.

Fredlund, D. G., Houston, S. L., Nguyen, Q., & Fredlund, M. D. (2010). Moisture movement through cracked clay soil profiles. *Geotechnical and Geological Engineering*, *28*(6), 865–888.

Gerke, H. H., Dusek, J., & Vogel, T. (2013). Solute mass transfer effects in two-dimensional dual-permeability modeling of bromide leaching from a tile-drained field. *Vadose Zone Journal*, *12*(2), 1–21.

Gerke, H. H., Dusek, J., Vogel, T., & Khne, J. M. (2007). Two-dimensional dual-permeability analyses of a bromide tracer experiment on a tile-drained field. *Vadose Zone Journal*, *6*(3), 651–667.

Gerke, H. H., & van Genuchten, M. T. (1993a). A dual-porosity model for simulating the preferential movement of water and solutes in structured porous media. *Water Resources Research*, *29*(2), 305–319.

Gerke, H. H., & van Genuchten, M. T. (1993b). Evaluation of a first-order water transfer term for variably saturated dual-porosity flow models. *Water Resources Research*, *29*(4), 1225–1238.
Gerke, H. H., & van Genuchten, M. T. (1996). Macroscopic representation of structural geometry for simulating water and solute movement in dual-porosity media. *Advances in Water Resources*, *19*(6), 343–357.
Germann, P. F., & Karlen, M. (2016). Viscous-flow approach to in situ infiltration and in vitro saturated hydraulic conductivity determination. *Vadose Zone Journal*, *15*(2), 1–15.
Ghanbarian-Alavijeh, B., Liaghat, A., Huang, G.-H., & van Genuchten, M. T. (2010). Estimation of the van Genuchten soil water retention properties from soil textural data. *Pedosphere*, *20*(4), 456–465.
Hendrickx, J. M. H., & Flury, M. (2001). Uniform and preferential flow mechanisms in the vadose zone. Conceptual models of flow and transport in the fractured vadose zone, 149–187.
Jarvis, N. (1994). The Macro Model (Version 3.1). technical description and sample simulations.
Köhne, J. M., Khne, S., & Šimůnek, J. (2009). A review of model applications for structured soils: a) Water flow and tracer transport. *Journal of Contaminant Hydrology*, *104*(1), 4–35.
Köhne, J. M., Mohanty, B. P., Šimůnek, J., & Gerke, H. H. (2004). Numerical evaluation of a second-order water transfer term for variably saturated dual-permeability models. *Water Resources Research*, *40*, W07409. https://doi.org/10.1029/2004WR003285
Li, J. H., & Zhang, L. M. (2010). Geometric parameters and REV of a crack network in soil. *Computers and Geotechnics*, *37*(4), 466–475.
Li, J. H., Zhang, L. M., & Li, X. (2011). Soil-water characteristic curve and permeability function for unsaturated cracked soil. *Canadian Geotechnical Journal*, *48*(7), 1010–1031.
Li, J. H., Zhang, L. M., Wang, Y., & Fredlund, D. G. (2009). Permeability tensor and representative elementary volume of saturated cracked soil. *Canadian Geotechnical Journal*, *46*(8), 928–942.
Moinfar, A., Narr, W., Hui, M.-H., Mallison, B. T., Lee, S. H., et al. (2011). Comparison of discrete-fracture and dual-permeability models for multiphase flow in naturally fractured reservoirs. In *Spe reservoir simulation symposium*, Society of Petroleum Engineers.
Morel-Seytoux, H. J., Meyer, P. D., Nachabe, M., Tourna, J., van Genuchten, M. T., & Lenhard, R. J. (1996). Parameter equivalence for the Brooks-Corey and van Genuchten soil characteristics: Preserving the effective capillary drive. *Water Resources Research*, *32*(5), 1251–1258.
Mualem, Y. (1976). A new model for predicting the hydraulic conductivity of unsaturated porous media. *Water Resources Research*, *12*(3), 513–522.
Novak, V., Šimůnek, J., & van Genuchten, M. T. (2000). Infiltration of water into soil with cracks. *Journal of Irrigation and Drainage Engineering*, *126*(1), 41–47.
Oron, A. P., & Berkowitz, B. (1998). Flow in rock fractures: The local cubic law assumption reexamined. *Water Resources Research*, *34*(11), 2811–2825.
Pouya, A. (2015). A finite element method for modeling coupled flow and deformation in porous fractured media. *International Journal for Numerical and Analytical Methods in Geomechanics*, *39*(16), 1836–1852.
Pouya, A., Vo, T. D., Hemmati, S., & Tang, A. M. (2019). Modeling soil desiccation cracking by analytical and numerical approaches. *International Journal for Numerical and Analytical Methods in Geomechanics*, *43*(3), 738–763.
Ray, C., Vogel, T., & Dusek, J. (2004). Modeling depth-variant and domain-specific sorption and biodegradation in dual-permeability media. *Journal of Contaminant Hydrology*, *70*(1), 63–87.
Samardzioska, T., & Popov, V. (2005). Numerical comparison of the equivalent continuum, non-homogeneous and dual porosity models for flow and transport in fractured porous media. *Advances in Water Resources*, *28*(3), 235–255.
Shao, W., Bogaard, T. A., Bakker, M., & Greco, R. (2015). Quantification of the influence of preferential flow on slope stability using a numerical modelling approach. *Hydrology and Earth System Sciences*, *19*(5), 2197–2212.
Snow, D. T. (1965). A parallel plate model of fractured permeable media.
Snow, D. T. (1969). Anisotropie permeability of fractured media. *Water Resources Research*, *5*(6), 1273–1289.
Song, L., Li, J., Garg, A., & Mei, G. (2018). Experimental study on water exchange between crack and clay matrix. *Geomechanics and Engineering*, *14*(3), 283–291.
Tinjum, J. M., Benson, C. H., & Blotz, L. R. (1997). Soil-water characteristic curves for compacted clays. *Journal of Geotechnical and Geoenvironmental Engineering*, *123*(11), 1060–1069.
van Genuchten, M. T. (1980). A closed-form equation for predicting the hydraulic conductivity of unsaturated soils. *Soil Science Society of America Journal*, *44*(5), 892–898.
van Lier, Q. J., & Pinheiro, E. A. R. (2018). An alert regarding a common misinterpretation of the van Genuchten α parameter. Revista Brasileira de Ciência do Solo, 42.
Vogel, T., Gerke, H. H., Zhang, R., & van Genuchten, M. T. (2000). Modeling flow and transport in a two-dimensional dual-permeability system with spatially variable hydraulic properties. *Journal of Hydrology*, *238*(1-2), 78–89.
Vogel, T., van Genuchten, M. T., & Cislerova, M. (2000). Effect of the shape of the soil hydraulic functions near saturation on variably-saturated flow predictions. *Advances in Water Resources*, *24*(2), 133–144.
Walton, K. M., Unger, A. ndreJ. A., Ioannidis, M. A., & Parker, B. L. (2019). Benchmarking napl redirection and matrix entry at fracture intersections below the water table. *Water Resources Research*, *55*, 2672–2689. https://doi.org/10.1029/2018WR023435
Wang, J. S. Y., & Narasimhan, T. N. (1985). Hydrologic mechanisms governing fluid flow in a partially saturated, fractured, porous medium. *Water Resources Research*, *21*(12), 1861–1874.
Wang, J. S. Y., & Narasimhan, T. N. (1993). Chapter 7: Unsaturated flow in fractured porous media. In J. Bear, C.-F. Tsang, & G. de Marsily (Eds.), *Flow and contaminant transport in fractured rock* (pp. 325–394). Oxford: Academic Press.
Whitaker, S. (1986). Flow in porous media I: A theoretical derivation of Darcy's law. *Transport in Porous Media*, *1*(1), 3–25.
Witherspoon, P. A., Wang, J. S. Y., Iwai, K., & Gale, J. E. (1980). Validity of cubic law for fluid flow in a deformable rock fracture. *Water Resources Research*, *16*(6), 1016–1024.
Šimůnek, J., Jarvis, N. J., van Genuchten, M. T., & Grdens, A. (2003). Review and comparison of models for describing non-equilibrium and preferential flow and transport in the vadose zone. *Journal of Hydrology*, *272*(1), 14–35.